



HAL
open science

The ALMA-PILS survey: First tentative detection of 3-hydroxypropenal (HOCHCHCHO) in the interstellar medium and chemical modeling of the C₃H₄O₂ isomers

A. Coutens, J.-C. Loison, A. Boulanger, E. Caux, H. S. P. Müller, V. Wakelam, S. Manigand, J. K. Jørgensen

► To cite this version:

A. Coutens, J.-C. Loison, A. Boulanger, E. Caux, H. S. P. Müller, et al.. The ALMA-PILS survey: First tentative detection of 3-hydroxypropenal (HOCHCHCHO) in the interstellar medium and chemical modeling of the C₃H₄O₂ isomers. *Astronomy and Astrophysics - A&A*, 2022, 660, pp.L6. 10.1051/0004-6361/202243038 . hal-03634712

HAL Id: hal-03634712

<https://hal.science/hal-03634712>

Submitted on 7 Apr 2022

HAL is a multi-disciplinary open access archive for the deposit and dissemination of scientific research documents, whether they are published or not. The documents may come from teaching and research institutions in France or abroad, or from public or private research centers.

L'archive ouverte pluridisciplinaire **HAL**, est destinée au dépôt et à la diffusion de documents scientifiques de niveau recherche, publiés ou non, émanant des établissements d'enseignement et de recherche français ou étrangers, des laboratoires publics ou privés.

LETTER TO THE EDITOR

The ALMA-PILS survey: First tentative detection of 3-hydroxypropenal (HOCHCHCHO) in the interstellar medium and chemical modeling of the C₃H₄O₂ isomers

A. Coutens¹, J.-C. Loison², A. Boulanger¹, E. Caux¹, H. S. P. Müller³, V. Wakelam⁴,
S. Manigand⁵, and J. K. Jørgensen⁶

¹ Institut de Recherche en Astrophysique et Planétologie (IRAP), Université de Toulouse, UPS, CNRS, CNES, 9 av. du Colonel Roche, 31028 Toulouse Cedex 4, France
e-mail: audrey.coutens@irap.omp.eu

² Institut des Sciences Moléculaires (ISM), CNRS, Université Bordeaux, 351 cours de la Libération, 33400 Talence, France

³ I. Physikalisches Institut, Universität zu Köln, Zùlpicher Str.77, 50937 Köln, Germany

⁴ Laboratoire d'astrophysique de Bordeaux, Univ. Bordeaux, CNRS, B18N, allée Geoffroy Saint-Hilaire, 33615 Pessac, France

⁵ Laboratoire d'Etudes Spatiales et d'Instrumentation en Astrophysique (LESIA), Observatoire de Paris, Université PSL, CNRS, Sorbonne Université, Université de Paris, 5 place Jules Janssen, 92195 Meudon, France

⁶ Niels Bohr Institute, University of Copenhagen, Øster Voldgade 5–7, 1350 Copenhagen K, Denmark

Received 4 January 2022 / Accepted 21 March 2022

ABSTRACT

Characterizing the molecular composition of solar-type protostars is useful for improving our understanding of the physico-chemical conditions under which the Sun and its planets formed. In this work, we analyzed the Atacama Large Millimeter/submillimeter Array (ALMA) data of the Protostellar Interferometric Line Survey (PILS), an unbiased spectral survey of the solar-type protostar IRAS 16293–2422, and we tentatively detected 3-hydroxypropenal (HOCHCHCHO) for the first time in the interstellar medium towards source B. Based on the observed line intensities and assuming local thermodynamic equilibrium, its column density is constrained to be $\sim 10^{15}$ cm⁻², corresponding to an abundance of 10^{-4} relative to methanol, CH₃OH. Additional spectroscopic studies are needed to constrain the excitation temperature of this molecule. We included HOCHCHCHO and five of its isomers in the chemical network presented in Manigand et al. (2021, A&A, 645, A53) and we predicted their chemical evolution with the Nautilus code. The model reproduces the abundance of HOCHCHCHO within the uncertainties. This species is mainly formed through the grain surface reaction CH₂CHO + HCO → HCOCH₂CHO, followed by the tautomerization of HCOCH₂CHO into HOCHCHCHO. Two isomers, CH₃COCHO and CH₂COHCHO, are predicted to be even more abundant than HOCHCHCHO. Spectroscopic studies of these molecules are essential in searching for them in IRAS 16293–2422 and other astrophysical sources.

Key words. astrochemistry – stars: formation – stars: protostars – ISM: molecules – ISM: individual objects: IRAS 16293–2422

1. Introduction

Characterizing the inventory of molecules in solar-type protostars is essential for gaining a better understanding of our origins, as such studies provide important clues about the chemical richness that was available at the time when the Sun and its planets formed. Large spectral surveys are ideal for identifying the variety of molecules present in these objects, which can lead to new molecular detections in space. Indeed, the number of first detections of molecules in the interstellar medium (ISM) continues to grow thanks to the improving capacities of the instruments in the centimeter, millimeter, and submillimeter range (McGuire 2022).

IRAS 16293–2422 (hereafter IRAS16293) is one of the most frequently studied solar-type protostars. The rich chemistry of this Class 0 protostellar system was studied in an unbiased way thanks to an array of large spectral surveys (e.g., IRAM-30m, JCMT, *Herschel*/HIFI, Caux et al. 2011; Ceccarelli et al. 2010). The Protostellar Interferometric Line Survey (PILS, Jørgensen et al. 2016), carried out with the Atacama Large

Millimeter/submillimeter Array (ALMA), has contributed significantly to the characterization of the chemical content in this source. It revealed, for the first time, the presence of various complex organics in solar-type protostars such as c-C₂H₄O, C₂H₅CHO, CH₃COCH₃, CH₃NCO, NH₂CN, CH₃NC, CH₃OCH₂OH, and t-C₂H₅OCH₃ (e.g., Lykke et al. 2017; Ligterink et al. 2017; Coutens et al. 2018; Calcutt et al. 2018; Manigand et al. 2020). Over the last few years, the first interstellar detections of CH₃Cl (Fayolle et al. 2017), HONO (Coutens et al. 2019), HOCH₂CN (Zeng et al. 2019), and CH₃C(O)CH₂OH (Zhou et al. 2020) were also obtained with ALMA towards component B of this source. More recently, Manigand et al. (2021) investigated the chemistry of three-carbon molecules in this protostar. This study led to the additional detection of propenal (C₂H₃CHO) and propylene (C₃H₆) in IRAS16293 B, while upper limits were derived for other species (C₃H₈, HCCCCHO, n-C₃H₇OH, i-C₃H₇OH, C₃O).

In this Letter, we report the first tentative interstellar detection of another three-carbon species, 3-hydroxypropenal (HOCHCHCHO) towards IRAS16293 B using the ALMA-PILS

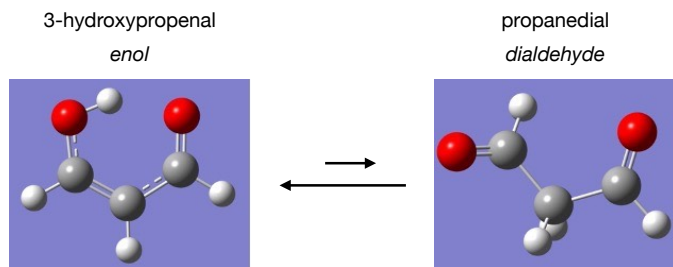


Fig. 1. Chemical representation of the tautomers of malonaldehyde. The enol form, 3-hydroxypropenal, is on the *left*, while the dialdehyde form, propanedial, is on the *right*.

data. This molecule is used as a biomarker to measure the level of oxidative stress in living organisms (e.g., Del Rio et al. 2005). It is produced via lipid peroxidation of polyunsaturated fatty acids (Pryor & Stanley 1975). The formation of this species in space is however unknown and, to our knowledge, it has never been predicted by astrochemical models. In the laboratory, $C_3H_4O_2$ was recently found to be produced in interstellar ice analogs of carbon monoxide and water at 5 K after the irradiation of energetic electrons, however, it was not possible to discriminate the isomer through the experiment (Turner et al. 2021).

This Letter is organized as follows. We present the PILS observations in Sect. 2. We analyze the data in Sect. 3. Finally, we present the chemical modeling of HOCHCHCHO and its isomers and we discuss the results in Sect. 4.

2. Observations and spectroscopy

The three-carbon species 3-hydroxypropenal is the enol tautomeric form of malonaldehyde. The enolic *cis* form is strongly favored over the dialdehyde form of malonaldehyde because of the ability to form an intramolecular hydrogen bond (see Fig. 1). The hydrogen atom of this bond can move fairly easily from the CH_2 group to the CHO group, thus exchanging the positions of the two groups. The tunneling is only slightly hindered, which leads to a splitting of 647 GHz ($\approx 21.6 \text{ cm}^{-1} \approx 31 \text{ K}$). The spectroscopic data of HOCHCHCHO come from the Cologne Database for Molecular Spectroscopy (CDMS, Müller et al. 2001, 2005). More information is available in Appendix A.

The ALMA/PILS survey is fully described in Jørgensen et al. (2016). In summary, these observations obtained with both the 12m array and the Atacama Compact Array (ACA) cover the entire range between 329.1 and 362.9 GHz (Band 7) with a resolution of 0.244 MHz ($\sim 0.2 \text{ km s}^{-1}$). The pointing center of the observations are taken to be in between IRAS16293A and IRAS16293B with both of them covered within the interferometric field of view. The sensitivity of the combined 12 m array and ACA observations is about $4\text{--}5 \text{ mJy beam}^{-1} \text{ km s}^{-1}$. The beam sizes vary between 0.4 and 0.7'' and the observations were restored with a circular beam of 0.5''. Besides the Band 7 observations, small spectral windows were also covered in Bands 3 and 6. More information about the data reduction, the continuum subtraction, and these additional data can be found in Jørgensen et al. (2016).

3. Analysis and results

Using a dedicated convolutional neural network (CNN) on a large set of multi-species synthetic spectra assuming local thermodynamic equilibrium (LTE, Boulanger et al. 2022), we pre-

dicted the presence of HOCHCHCHO in the PILS data with a probability greater than 50%. The applied spectrum corresponds to the component B of IRAS16293 at a position offset by 0.5'' (one beam) with respect to the continuum peak position in the south-west direction ($\alpha_{J2000} = 16^{\text{h}}32^{\text{m}}22^{\text{s}}.58$, $\delta_{J2000} = -24^{\circ}28'32.8''$). This position is regularly used in the PILS studies to search for molecules and isotopologues, as the lines are relatively narrow ($FWHM \sim 1 \text{ km s}^{-1}$) and bright without being affected by absorption features (e.g., Coutens et al. 2016; Lykke et al. 2017). We confirm that several lines can be identified as HOCHCHCHO with a classical analysis using the CASSIS¹ software. As the lines are broader towards IRAS16293 A, it is not possible to identify isolated transitions of 3-hydroxypropenal toward that source.

Our analysis is similar to those presented in earlier studies (e.g., Coutens et al. 2016, 2019; Lykke et al. 2017; Ligerink et al. 2017). Synthetic spectra are produced assuming LTE for various values of column densities, N , and excitation temperatures, T_{ex} . A χ^2 method is then used on the unblended lines to derive the best fit parameters. To ensure that the lines are not blended with other species, we overlaid the model including the species previously identified in this source. We added HONO (Coutens et al. 2019), CH_3OCH_2OH , CH_2DCHO , $t\text{-}C_2H_5OCH_3$ (Manigand et al. 2020), C_2H_3CHO , C_3H_6 (Manigand et al. 2021), and CH_3OCHD_2 (Richard et al. 2021) to the list presented in Appendix A of Coutens et al. (2019). We excluded from the analysis all the transitions with large uncertainties according to the spectroscopy (see Appendix A) those that are significantly blended with other species as well as a few that were affected by absorption features (see Table B.4). In total, we found 11 lines ($\geq 20 \text{ mJy beam}^{-1}$) that could be associated to HOCHCHCHO towards IRAS16293 B (see Fig. 2, Tables 1 and B.1).

To constrain the best-fit parameters, we ran two grids: one with large steps followed by another one around the best model with smaller steps ($\Delta N = 2 \times 10^{14} \text{ cm}^{-2}$, $\Delta T = 25 \text{ K}$). For this second grid, the column density ranged from 2×10^{14} to $3 \times 10^{15} \text{ cm}^{-2}$, while the excitation temperature was between 50 and 350 K. To avoid overestimating the column density, we also included five undetected lines presenting small uncertainties in the χ^2 analysis (see Table B.2). The best-fit model was obtained for a column density N of $2.2 \times 10^{15} \text{ cm}^{-2}$ and an excitation temperature T_{ex} of 350 K ($\chi_{\text{red}}^2 \sim 2.0$). However, the excitation temperature was not well constrained. Our χ^2 analysis shows that various models with excitation temperatures in the 75–350 K range can properly reproduce the lines included in the calculation (3σ uncertainty). It is due to the E_{up} values of the detected lines that only span a small range (see Tables 1 and B.2). Indeed, transitions with higher E_{up} values are present in the PILS range but they all show large uncertainties and are consequently excluded from the analysis. Previous molecules identified in the PILS survey were classified in two categories according to their excitation temperatures. For some molecules, the excitation temperature is found to be $\sim 125 \text{ K}$ while for others, it is $\sim 300 \text{ K}$ (see Jørgensen et al. 2018 for more details). If we assume excitation temperatures of 125 and 300 K, we obtain column densities of 3-hydroxypropenal of $1.0 \times 10^{15} \text{ cm}^{-2}$ ($\chi_{\text{red}}^2 \sim 2.0$) and $1.8 \times 10^{15} \text{ cm}^{-2}$ ($\chi_{\text{red}}^2 \sim 2.0$), respectively. In the second hypothesis ($\geq 300 \text{ K}$), tens of additional lines should be detected. Given their large uncertainties, it is usually easy to find lines within the uncertainties that could be reproduced by the models with

¹ CASSIS has been developed by IRAP-UPS/CNRS (Vastel et al. 2015). <http://cassis.irap.omp.eu/>

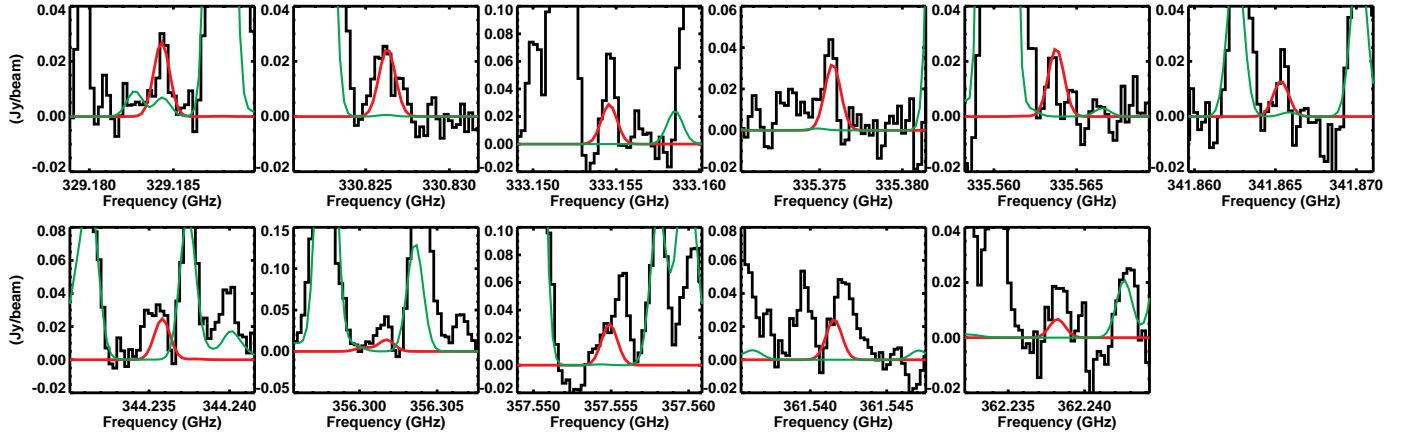


Fig. 2. Lines identified as HOCHCHCHO towards IRAS16293 B. The observations are in black. The model with $N = 1.0 \times 10^{15} \text{ cm}^{-2}$ and $T_{\text{ex}} = 125 \text{ K}$ is overlaid in red. The green line corresponds to the model which includes the previous molecules identified in the PILS survey. The lines at 333.1545, 341.8653, 356.3017, and 362.2382 GHz could be partially blended with unknown species.

Table 1. Transitions identified as HOCHCHCHO towards IRAS 16293 B.

Transition				Frequency	Uncertainty	E_{up}	A_{ij}	g_{up}
N'	K'_a	K'_c	$v'_t - N''$	(MHz)	(MHz)	(K)	(s^{-1})	
17	17	0	1 - 16 16 1 1	329184.2911	0.0223	171.1	1.30×10^{-3}	35
17	17	1	1 - 16 16 0 1	329184.2911	0.0223	171.1	1.29×10^{-3}	105
21	14	7	0 - 20 13 8 0	330826.2042	0.0188	148.7	8.32×10^{-4}	129
21	14	8	0 - 20 13 7 0	330826.5149	0.0188	148.7	8.32×10^{-4}	43
20	15	5	0 - 19 14 6 0 ^(†)	333154.5692	0.0155	147.3	9.76×10^{-4}	41
20	15	6	0 - 19 14 5 0 ^(†)	333154.5726	0.0155	147.3	9.76×10^{-4}	123
19	16	3	0 - 18 15 4 0	335375.7805	0.0154	146.9	1.14×10^{-3}	117
19	16	4	0 - 18 15 3 0	335375.7805	0.0154	146.9	1.14×10^{-3}	39
19	16	3	1 - 18 15 4 1	335563.7519	0.0154	177.9	1.12×10^{-3}	39
19	16	4	1 - 18 15 3 1	335563.7519	0.0154	177.9	1.12×10^{-3}	117
25	12	13	0 - 24 11 14 0 ^(†)	341865.3358	0.0411	176.0	5.78×10^{-4}	153
20	16	4	1 - 19 15 5 1	344235.8096	0.0157	186.3	1.14×10^{-3}	123
20	16	5	1 - 19 15 4 1	344235.8096	0.0157	186.3	1.14×10^{-3}	41
24	14	10	1 - 23 13 11 1 ^(†)	356301.7349	0.0304	208.6	8.58×10^{-4}	147
19	18	1	1 - 18 17 2 1	357554.8901	0.0231	195.8	1.56×10^{-3}	39
19	18	2	1 - 18 17 1 1	357554.8901	0.0231	195.8	1.56×10^{-3}	117
22	16	7	1 - 21 15 6 1	361541.5437	0.0191	204.3	1.18×10^{-3}	45
22	16	6	1 - 21 15 7 1	361541.5438	0.0191	204.3	1.18×10^{-3}	135
29	12	18	1 - 28 11 17 1 ^(†)	362238.2039	0.0768	253.7	4.87×10^{-4}	177

Notes. ^(†)The best-fit model only reproduces half of the line fluxes. These lines could consequently be partially blended with unknown species.

high T_{ex} . However, there are a few exceptions for the transitions at 343.4656, 349.9189, and 350.0168 GHz that do not show lines within their uncertainties, which suggests that the excitation temperature could be lower than 300 K. Additional spectroscopic measurements would be needed to definitely answer this question. The model predictions obtained for $T_{\text{ex}} = 125 \text{ K}$ are overlaid on the spectra of the detected lines in Fig. 2 and the undetected ones in Fig. B.1. Seven lines are correctly reproduced by the model and can be identified as HOCHCHCHO. The lines at 333.1546, 341.8653, 356.3017, and 362.2382 GHz are only partially reproduced, which could mean that they are partially blended with unknown species. We carefully checked that no HOCHCHCHO line is missing with this model in other parts of the PILS survey. In Band 6, two faint lines are detected at 247.5312 and 250.4599 GHz and are in agreement with the model. Another feature is present at 239.4605 GHz but blended

with an unidentified species (see Fig. B.2). No line is found in Band 3.

The moment 0 maps of the transitions at 329.1843, 330.8262, and 335.3758 GHz are presented in Fig. B.4. The emission is compact and similar to the other COMs detected in this source (see e.g., Lykke et al. 2017; Jørgensen et al. 2018; Calcutt et al. 2018).

The isomers of 3-hydroxypropenal were also searched for in the PILS data. HCOCH₂CHO (propanedial), CH₃COCHO (methylglyoxal), and CH₂COHCHO (2-hydroxypropenal) are not in the spectroscopic databases CDMS and JPL (Pickett et al. 1998). Only C₂H₃OCHO (vinyl formate) and the *s*-cis and *s*-trans conformers of C₂H₃COOH (propenoic acid) are available in CDMS. C₂H₃OCHO is not detected with an upper limit of $4 \times 10^{15} \text{ cm}^{-2}$ based on the undetected transition at 355.2462 GHz. Upper limits of $1 \times 10^{15} \text{ cm}^{-2}$ and

Table 2. Predicted and observed abundances of the C₃H₄O₂ isomers.

Isomer	Formula	Predicted abundance (/H)	Predicted abundance (/CH ₃ OH)	Observed abundance (/CH ₃ OH)
3-Hydroxypropenal	HOCHCHCHO	1.4×10^{-8}	4.6×10^{-4}	1.0×10^{-4}
Propanedial	HCOCH ₂ CHO	3.0×10^{-9}	9.9×10^{-5}	
Methyl glyoxal	CH ₃ COCHO	7.4×10^{-8}	2.4×10^{-3}	
2-Hydroxypropenal	CH ₂ COHCHO	2.0×10^{-8}	6.6×10^{-4}	
Vinyl formate	C ₂ H ₃ OCHO	8.4×10^{-10}	2.8×10^{-5}	$\leq 4 \times 10^{-4}$
2-Propenoic acid	C ₂ H ₃ COOH	2.2×10^{-13}	7.3×10^{-9}	$\leq 5 \times 10^{-4}$

Notes. The total uncertainty on the predicted abundances is about a factor 10.

$4 \times 10^{15} \text{ cm}^{-2}$ are also derived for the s-cis and s-trans conformers of C₂H₃COOH, respectively.

If 3-hydroxypropenal forms on grains, its hydrogenation could potentially lead to the saturated version, 1,3-propanediol (CH₂OHCH₂CH₂OH). Indeed, many saturated COMs have been detected towards IRAS16293. The lower energy conformer a'GG'g present in the CDMS database was searched for and an upper limit of $1 \times 10^{15} \text{ cm}^{-2}$ was derived.

4. Chemical modeling and discussion

To better understand the chemistry of HOCHCHCHO and its isomers, we used the Nautilus code (Ruaud et al. 2016), a three-phase gas, grain surface, and grain mantle time-dependent chemical model. We updated the chemical network described in Manigand et al. (2021) by including the reactions producing and consuming the C₃H₄O₂ isomers as well as some radical species linked to C₃H₄O₂ and not yet present in the network, for example CH₂CHO, CH₂COH, or HCCHOH (see Appendix C). For the physical model of the formation of a low-mass protostar, we considered two successive stages, similarly to Manigand et al. (2021): (i) a uniform and constant stage, corresponding to the pre-stellar phase, with a density of $5 \times 10^4 \text{ cm}^{-3}$, a temperature of 10 K for both gas and dust, a visual extinction of 4.5 mag, a cosmic-ray ionization rate of $1.3 \times 10^{-17} \text{ s}^{-1}$, a standard external UV field of 1 G₀, the initial abundances listed in Table 3 of Manigand et al. (2021), and a duration of 10^6 years; and (ii) the collapse phase described in Manigand et al. (2021).

Six C₃H₄O₂ isomers are introduced in the network: 3-hydroxypropenal (HOCHCHCHO), 2-propenoic acid (C₂H₃COOH), methyl glyoxal (CH₃COCHO), propanedial (HCOCH₂CHO), 2-hydroxypropenal (CH₂COHCHO), and vinyl formate (C₂H₃OCHO). The description of their formation and destruction pathways is presented in Appendix C. HOCHCHCHO is mainly formed through an indirect way through the reaction CH₂CHO + HCO → HCOCH₂CHO followed by the tautomerization of HCOCH₂CHO into HOCHCHCHO. The predicted abundances with respect to CH₃OH are indicated in Table 2. Among the different isomers of C₃H₄O₂, three are relatively abundant according to the model. HOCHCHCHO has a predicted abundance with respect to CH₃OH of 4.6×10^{-4} in agreement with the observations (1×10^{-4}) (see below for the discussions on uncertainties). In addition, CH₃COCHO and CH₂COHCHO also show high abundances (with respect to CH₃OH) of 2×10^{-3} and 6×10^{-4} , respectively. Future detections could be possible for these two species if the spectroscopic data are available. It should be noted that the calculated structure of propanedial (HCOCH₂CHO) is non-planar. Its dipole moment is very uncertain because it

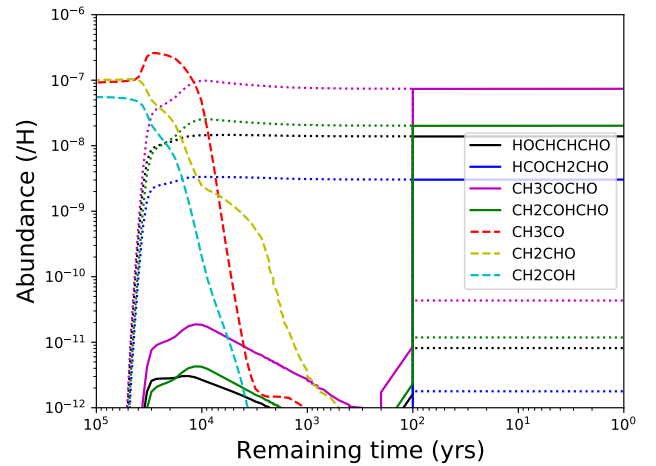


Fig. 3. Evolution of the abundances of the C₃H₄O₂ isomers, HOCHCHCHO, HCOCH₂CHO, CH₃COCHO, and CH₂COHCHO, and their precursors, CH₃CO, CH₂CHO, and CH₂COH, during the collapse phase. Solid and dotted lines are used to indicate the gas phase and grain mantle + surface abundances of the C₃H₄O₂ isomers, respectively. Dashed lines are used to represent the grain mantle + surface abundances of the precursors.

depends strongly on the dihedral angle between the two -CHO groups². Consequently, HCOCH₂CHO which is predicted to have a relatively high abundance (with respect to CH₃OH) of 1×10^{-4} may be also detectable. Figure 3 shows the evolution of the most abundant isomers and their precursors during the collapse phase.

The formation pathways of CH₃COCHO, particularly the grain surface reaction CH₃CO + HCO, are credible and the calculated abundance of CH₃COCHO makes it a potentially detectable species. For CH₂COHCHO, it is more ambiguous because one of the main pathways of formation is the isomerization of CH₃COCHO, which could be very less favorable on grains that the result given by the methodology used here. The abundances of C₃H₄O₂ isomers are linearly dependent on the branching ratios of the association reactions, which are not known but whose uncertainty can be estimated at about a factor of 2 in this case. The abundances are also highly sensitive to the reactions with hydrogen atoms, which are the most efficient destruction reactions in our model. The barriers were calculated using the DFT method associated with the M06-2X functional. As these reactions take place through tunneling, they are dependent on the barrier time and the barrier width estimated by calculating the imaginary frequency. The uncertainty on the rate

² <https://cccbdb.nist.gov/dipole2x.asp>

of these reactions is therefore not negligible and the uncertainty induced on the $C_3H_4O_2$ abundances can be estimated to be about a factor of 5. Thus, the total uncertainty on the predicted abundances of the $C_3H_4O_2$ isomers is about a factor of 10.

In conclusion, this study confirms that solar-type protostars can harbor a broad variety of complex organic molecules in their warm inner regions, highlighting the importance of additional spectroscopic studies of three-carbon species in the submillimeter range.

Acknowledgements. This paper makes use of the ALMA data ADS/JAO.ALMA#2013.1.00278.S and ADS/JAO.ALMA#2012.1.00712.S. ALMA is a partnership of ESO (representing its member states), NSF (USA) and NINS (Japan), together with NRC (Canada) and NSC and ASIAA (Taiwan), in cooperation with the Republic of Chile. The Joint ALMA Observatory is operated by ESO, AUI/NRAO, and NAOJ. This project has received funding from the European Research Council (ERC) under the European Union's Horizon 2020 research and innovation programme (grant agreement 949278, Chemtrip). V.W. acknowledges the CNRS program "Physique et Chimie du Milieu Interstellaire" (PCMI) co-funded by the Centre National d'Etudes Spatiales (CNES). J.K.J. acknowledges support from the Independent Research Fund Denmark (grant No. DFF0135-00123B).

References

- Anastasi, C., & Maw, P. R. 1982, *J. Chem. Soc.*, 78, 2423
- Baba, T., Tanaka, T., Morino, I., Yamada, K. M. T., & Tanaka, K. 1999, *J. Chem. Phys.*, 110, 4131
- Baughcum, S. L. 1983, Ph.D. Thesis, Harvard University, Cambridge MA, USA
- Baughcum, S., Duerst, R., Rowe, W., Smith, Z., & Wilson, E. 1981, *J. Am. Chem. Soc.*, 103, 6296
- Baulch, D. L., Bowman, C. T., Cobos, C. J., et al. 2005, *J. Phys. Chem. Ref. Data*, 34, 757
- Boulangier, A., Caux, E., & Dupin de Saint-Cyr, F. 2022, *Astronomical Data Analysis Software and Systems XXXI*, submitted
- Calcutt, H., Fiechter, M. R., Willis, E. R., et al. 2018, *A&A*, 617, A95
- Caux, E., Kahane, C., Castets, A., et al. 2011, *A&A*, 532, A23
- Ceccarelli, C., Bacmann, A., Boogert, A., et al. 2010, *A&A*, 521, L22
- Coutens, A., Jørgensen, J. K., van der Wiel, M. H. D., et al. 2016, *A&A*, 590, L6
- Coutens, A., Willis, E. R., Garrod, R. T., et al. 2018, *A&A*, 612, A107
- Coutens, A., Ligterink, N. F. W., Loison, J. C., et al. 2019, *A&A*, 623, L13
- Del Rio, D., Stewart, A. J., & Pellegrini, N. 2005, *Nutr Metab Cardiovasc Dis.*, 15, 316
- Ding, Y.-H., Zhang, X., Li, Z.-S., Huang, X.-R., & Sun, C.-C. 2001, *J. Phys. Chem. A*, 105, 8206
- Fayolle, E. C., Öberg, K. I., Jørgensen, J. K., et al. 2017, *Nat. Astron.*, 1, 703
- Firth, D., Beyer, K., Dvorak, M., et al. 1991, *J. Chem. Phys.*, 94, 1812
- Garrod, R. T. 2013, *ApJ*, 765, 60
- Garrod, R. T., Belloche, A., Müller, H. S. P., & Menten, K. M. 2017, *A&A*, 601, A48
- Guthrie, J. P. 1978, *Can. J. Chem.*, 56, 962
- Harada, N., Herbst, E., & Wakelam, V. 2010, *ApJ*, 721, 1570
- Herbst, E., Terzieva, R., & Talbi, D. 2000, *MNRAS*, 311, 869
- Hippler, H., & Viskolcz, B. L. 2002, *Phys. Chem. Chem. Phys. (Incorporating Faraday Trans.)*, 4, 4663
- Jørgensen, J. K., van der Wiel, M. H. D., Coutens, A., et al. 2016, *A&A*, 595, A117
- Jørgensen, J. K., Müller, H. S. P., Calcutt, H., et al. 2018, *A&A*, 620, A170
- Jung, S.-H., Jang, S.-C., Kim, J.-W., Kim, J.-W., & Choi, J.-H. 2015, *J. Phys. Chem. A*, 119, 11761
- Ligterink, N. F. W., Coutens, A., Kofman, V., et al. 2017, *MNRAS*, 469, 2219
- Lykke, J. M., Coutens, A., Jørgensen, J. K., et al. 2017, *A&A*, 597, A53
- Manigand, S., Jørgensen, J. K., Calcutt, H., et al. 2020, *A&A*, 635, A48
- Manigand, S., Coutens, A., Loison, J. C., et al. 2021, *A&A*, 645, A53
- McGuire, B. A. 2022, *ApJS*, 259, 30
- Michael, J. V., Nava, D. F., Payne, W. A., & Stief, L. J. 1979, *J. Chem. Phys.*, 70, 5222
- Minissale, M., Dulieu, F., Cazaux, S., & Hocuk, S. 2016, *A&A*, 585, A24
- Moulds, L. d. V., & Riley, H. L. 1938, *J. Chem. Soc.*, 1938, 621
- Müller, H. S. P., Thorwirth, S., Roth, D. A., & Winnewisser, G. 2001, *A&A*, 370, L49
- Müller, H. S. P., Schlöder, F., Stutzki, J., & Winnewisser, G. 2005, *J. Mol. Struct.*, 742, 215
- Pickett, H. M., Poynter, R. L., Cohen, E. A., et al. 1998, *J. Quant. Spectr. Rad. Transf.*, 60, 883
- Pryor, W. A., & Stanley, J. P. 1975, *J. Org. Chem.*, 40, 3615
- Richard, C., Jørgensen, J. K., Margulès, L., et al. 2021, *A&A*, 651, A120
- Ruau, M., Wakelam, V., & Hersant, F. 2016, *MNRAS*, 459, 3756
- Senosiain, J. P., Klippenstein, S. J., & Miller, J. A. 2006, *J. Phys. Chem. A*, 110, 5772
- Stolze, M., Hübner, D., & Sutter, D. 1983, *J. Mol. Struct.*, 97, 243
- Turner, P., Baughcum, S., Coy, S., & Smith, Z. 1984, *J. Am. Chem. Soc.*, 106, 2265
- Turner, A. M., Bergantini, A., Koutsogiannis, A. S., et al. 2021, *ApJ*, 916, 74
- Vastel, C., Bottinelli, S., Caux, E., Glorian, J. M., & Boiziot, M. 2015, *SF2A-2015: Proceedings of the Annual meeting of the French Society of Astronomy and Astrophysics*, 313
- Wakelam, V., Loison, J. C., Mereau, R., & Ruau, M. 2017, *Mol. Astrophys.*, 6, 22
- Whytock, D. A., Michael, J. V., Payne, W. A., & Stief, L. J. 1976, *J. Chem. Phys.*, 65, 4871
- Zeng, S., Quénard, D., Jiménez-Serra, I., et al. 2019, *MNRAS*, 484, L43
- Zhou, Y., Quan, D.-H., Zhang, X., & Qin, S.-L. 2020, *Res. Astron. Astrophys.*, 20, 125

Appendix A: Spectroscopy of 3-hydroxypropenal

The spectroscopy of 3-hydroxypropenal is based on the measurements reported in Baughcum (1983), Stolze et al. (1983), Turner et al. (1984), Firth et al. (1991), and Baba et al. (1999). The b-dipole moment component comes from Baughcum et al. (1981) while the a-dipole moment was determined by Baba et al. (1999). The strong *b*-type transitions occur within the tunneling states (rotational transitions), whereas the weak *a*-type transitions connect the two tunneling states (rotation-tunneling transitions). The extensive set of experimental rotational transitions cover a large range of *J* quantum numbers; however, transitions with the lowest K_a were only accessed for low values of *J* as these are somewhat weaker than higher- K_a transitions in the same range. In addition, the small amount of rotation-tunneling transitions have also high values of K_a . Therefore, transitions having high values of *J* and very low values of K_a have large uncertainties which prohibit their unambiguous identification in the ALMA/PILS data sets cur-

rently, even though their intensities should be sufficiently above the noise limit in at least some cases.

Appendix B: Additional tables and figures

Table B.1 lists the observational parameters of the detected HOCHCHCHO lines obtained after Gaussian fitting. The undetected transitions of HOCHCHCHO used in the calculations presented in Section 3 (see Table B.2) are shown in Fig. B.1. The additional lines detected in Band 6 (see Table B.3) are shown in Fig. B.2. The other transitions of HOCHCHCHO that are either blended or affected by absorption features (see Table B.4) are shown in Fig. B.3. The model that includes the previously detected molecules (in green) is known to overproduce the intensities of optically thick lines. The spectroscopy can also be uncertain in some cases. Maps of three HOCHCHCHO transitions are shown in Fig. B.4.

Table B.1. Observed line parameters of the HOCHCHCHO transitions identified towards IRAS 16293 B.

Transition		Frequency	Integrated flux	I_{\max}	v_{LSR}	$FWHM$
N'	$K'_a K'_c v'_t - N'' K''_a K''_c v''_t$	(MHz)	(Jy beam ⁻¹ km s ⁻¹)	(Jy beam ⁻¹)	(km s ⁻¹)	(km s ⁻¹)
17	17 0 1 - 16 16 1 1	329184.3	0.024	0.028 ± 0.004	2.64 ± 0.05	0.72 ± 0.11
17	17 1 1 - 16 16 0 1	329184.3				
21	14 7 0 - 20 13 8 0	330826.2	0.037	0.022 ± 0.003	2.76 ± 0.08	1.61 ± 0.21
21	14 8 0 - 20 13 7 0	330826.5				
20	15 5 0 - 19 14 6 0 †	333154.6	0.045	0.069 ± 0.007	2.66 ± 0.03	0.63 ± 0.07
20	15 6 0 - 19 14 5 0 †	333154.6				
19	16 3 0 - 18 15 4 0	335375.8	0.032	0.045 ± 0.006	2.88 ± 0.05	0.70 ± 0.11
19	16 4 0 - 18 15 3 0	335375.8				
19	16 3 1 - 18 15 4 1	335563.8	0.016	0.024 ± 0.005	2.95 ± 0.05	0.51 ± 0.12
19	16 4 1 - 18 15 3 1	335563.8				
25	12 13 0 - 24 11 14 0 †	341865.3	0.014	0.025 ± 0.005	2.60 ± 0.04	0.47 ± 0.10
20	16 4 1 - 19 15 5 1 ‡	344235.8	0.020	0.033 ± 0.003	2.81 ± 0.09	0.76 ± 0.19
20	16 5 1 - 19 15 4 1 ‡	344235.8				
24	14 10 1 - 23 13 11 1 †	356301.7	0.032	0.040 ± 0.006	2.87 ± 0.06	0.78 ± 0.14
19	18 1 1 - 18 17 2 1 ‡	357554.9	< 0.067	0.026 ± 0.003	2.89 ± 0.15	1.10 ± 0.35
19	18 2 1 - 18 17 1 1 ‡	357554.9				
22	16 7 1 - 21 15 6 1 ‡	361541.5	< 0.045	0.023 ± 0.031	[2.7]	[0.7]
22	16 6 1 - 21 15 7 1 ‡	361541.5				
29	12 18 1 - 28 11 17 1 †	362238.2	0.019	0.020 ± 0.003	2.62 ± 0.07	0.96 ± 0.16
13	12 1 1 - 12 11 2 1 ‡	239460.6	< 0.020	0.008 ± 0.003	[2.7]	[0.7]
13	12 2 1 - 12 11 1 1 ‡	239460.6				
18	9 10 0 - 17 8 9 0	247531.2	0.012	0.011 ± 0.001	2.59 ± 0.06	1.19 ± 0.17
13	13 0 1 - 12 12 1 1	250459.9	0.012	0.015 ± 0.001	2.43 ± 0.05	0.87 ± 0.13
13	13 1 1 - 12 12 0 1	250459.9				

Note: The values in square brackets are assumed. The uncertainties correspond to the fit uncertainties only. † These lines could be partially blended with unknown species. ‡ A double Gaussian is used to fit the observations.

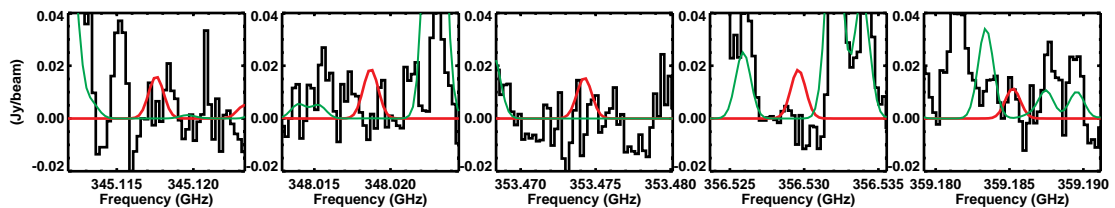


Fig. B.1. Observations of the undetected HOCHCHCHO transitions used in the χ^2 analysis (black). The model with $N = 1.0 \times 10^{15}$ cm⁻² and $T_{\text{ex}} = 125$ K is overlaid in red. The green line corresponds to the model including the previous molecules identified in the PILS survey.

Table B.2. List of the undetected transitions of HOCHCHCHO used in the χ^2 analysis.

Transition		Frequency	Uncertainty	E_{up}	A_{ij}	g_{up}
$N' K'_a K'_c v'_t - N'' K''_a K''_c v''_t$		(MHz)	(MHz)	(K)	(s^{-1})	
24 13 12 0 - 23 12 11 0		345117.5624	0.0325	171.4	7.24×10^{-4}	147
23 14 9 0 - 22 13 10 0		348018.6951	0.0263	167.9	8.64×10^{-4}	141
25 13 12 0 - 24 12 13 0		353474.2386	0.0377	182.1	7.34×10^{-4}	153
24 14 11 0 - 23 13 10 0		356529.5940	0.0301	178.2	8.87×10^{-4}	147
27 12 15 0 - 26 11 16 0		359185.2111	0.0572	199.1	5.72×10^{-4}	165

Table B.3. List of the transitions identified as HOCHCHCHO in Band 6.

Transition		Frequency	Uncertainty	E_{up}	A_{ij}	g_{up}
$N' K'_a K'_c v'_t - N'' K''_a K''_c v''_t$		(MHz)	(MHz)	(K)	(s^{-1})	
13 12 1 1 - 12 11 2 1		239460.5534	0.0102	107.0	4.43×10^{-4}	27
13 12 2 1 - 12 11 1 1		239460.5534	0.0102	107.0	4.43×10^{-4}	81
18 9 10 0 - 17 8 9 0		247531.1948	0.0167	93.9	2.26×10^{-4}	111
13 13 0 1 - 12 12 1 1		250459.9239	0.0124	113.6	5.59×10^{-4}	27
13 13 1 1 - 12 12 0 1		250459.9239	0.0124	113.6	5.59×10^{-4}	81

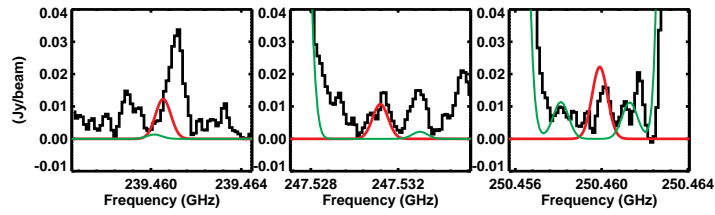
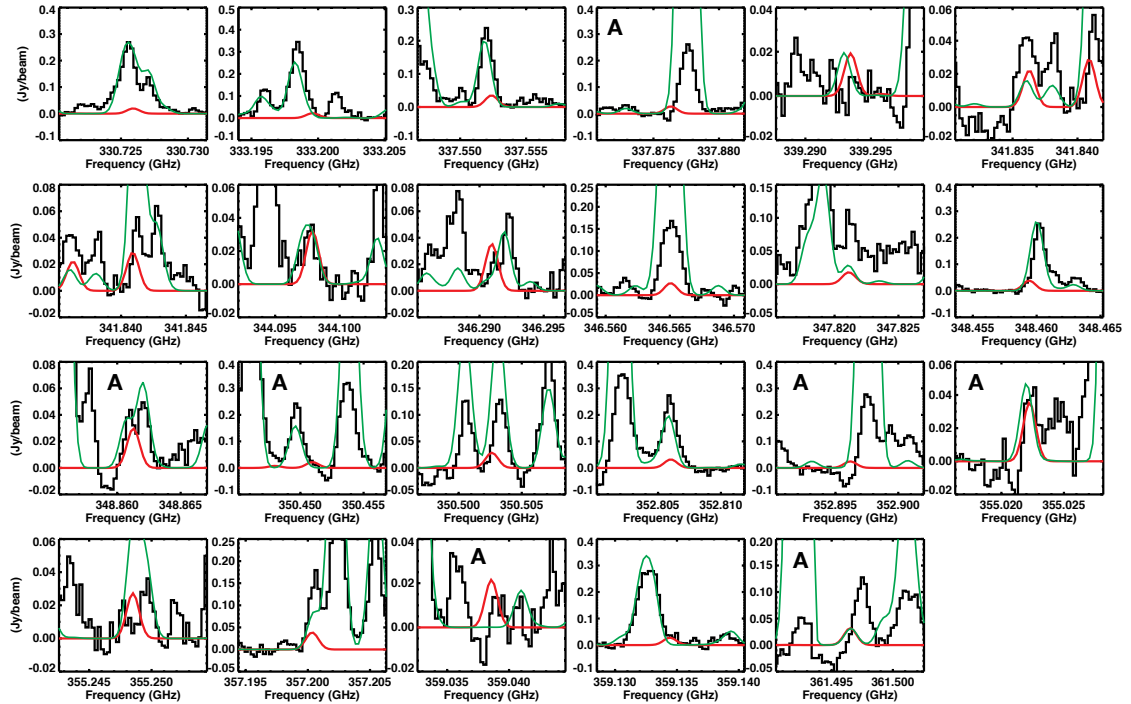

Fig. B.2. Lines of HOCHCHCHO identified in Band 6 (black). The model with $N = 1.0 \times 10^{15} \text{ cm}^{-2}$ and $T_{\text{ex}} = 125 \text{ K}$ is overlaid in red. The green line corresponds to the model including the previous molecules identified in the PILS survey.

Fig. B.3. Observations of the other HOCHCHCHO transitions that are blended and/or affected by absorption features (black). The Letter A is added on the panel where significant absorption features are seen at the half-beam offset position. The model with $N = 1.0 \times 10^{15} \text{ cm}^{-2}$ and $T_{\text{ex}} = 125 \text{ K}$ is overlaid in red. The green line corresponds to the model including the previous molecules identified in the PILS survey.

Table B.4. List of the HOCHCHCHO transitions excluded from the analysis due to blending with other species or absorption features.

Transition	Frequency (MHz)	Uncertainty (MHz)	E_{up} (K)	A_{ij} (s^{-1})	g_{up}	Reason for exclusion
21 14 8 1 - 20 13 7 1	330725.9000	0.0187	179.4	8.11×10^{-4}	129	Blended with C ₂ H ₅ OH
21 14 7 1 - 20 13 8 1	330725.9273	0.0187	179.4	8.1×10^{-4}	43	and CH ₃ COCH ₃
20 15 6 1 - 19 14 5 1	333199.5740	0.0154	178.2	9.56×10^{-4}	41	Blended with CH ₂ DOCH ₃
20 15 5 1 - 19 14 6 1	333199.5741	0.0154	178.2	9.56×10^{-4}	123	
18 17 1 0 - 17 16 2 0	337552.3721	0.0200	147.5	1.32×10^{-3}	37	Blended with D ₂ ¹³ CO
18 17 2 0 - 17 16 1 0	337552.3721	0.0200	147.5	1.32×10^{-3}	111	
18 17 2 1 - 17 16 1 1	337876.3115	0.0200	178.7	1.31×10^{-3}	37	Blended with CH ₃ OH
18 17 1 1 - 17 16 2 1	337876.3115	0.0200	178.7	1.31×10^{-3}	111	+ Absorption
22 14 9 1 - 21 13 8 1	339293.3621	0.0219	188.7	8.27×10^{-4}	45	Blended with NHDCN
22 14 8 1 - 21 13 9 1	339293.4748	0.0219	188.7	8.27×10^{-4}	135	
21 15 6 1 - 20 14 7 1	341836.2789	0.0175	187.0	9.75×10^{-4}	129	Blended with ¹³ CH ₃ OH
21 15 7 1 - 20 14 6 1	341836.2797	0.0175	187.0	9.75×10^{-4}	43	
21 15 6 0 - 20 14 7 0	341840.8890	0.0176	156.2	9.99×10^{-4}	129	Blended with CH ₃ OCHO
21 15 7 0 - 20 14 6 0	341840.9043	0.0176	156.2	9.99×10^{-4}	43	
20 16 5 0 - 19 15 4 0	344097.8858	0.0157	155.4	1.16×10^{-3}	123	Blended with CH ₃ OCHO
20 16 4 0 - 19 15 5 0	344097.8858	0.0157	155.4	1.16×10^{-3}	41	
19 17 2 0 - 18 16 3 0	346290.9455	0.0183	155.5	1.35×10^{-3}	117	Blended with CH ₂ DOH
19 17 3 0 - 18 16 2 0	346290.9455	0.0183	155.5	1.35×10^{-3}	39	
19 17 2 1 - 18 16 3 1	346565.0565	0.0183	186.6	1.33×10^{-3}	39	Blended with C ₂ H ₅ OH
19 17 3 1 - 18 16 2 1	346565.0565	0.0183	186.6	1.33×10^{-3}	117	and CH ₃ OCHO
23 14 10 1 - 22 13 9 1	347821.0130	0.0258	198.4	8.43×10^{-4}	141	Blended with (CH ₂ OH) ₂
23 14 9 1 - 22 13 10 1	347821.4373	0.0258	198.4	8.43×10^{-4}	47	
18 18 0 0 - 17 17 1 0	348459.4070	0.0257	156.7	1.56×10^{-3}	37	Blended with CH ₂ DCHO
18 18 1 0 - 17 17 0 0	348459.4070	0.0257	156.7	1.56×10^{-3}	111	
18 18 0 1 - 17 17 1 1	348861.2642	0.0258	187.9	1.55×10^{-3}	111	Blended with CH ₃ OCHO and
18 18 1 1 - 17 17 0 1	348861.2642	0.0258	187.9	1.55×10^{-3}	37	CH ₂ DOCHO + Absorption
22 15 8 1 - 21 14 7 1	350450.9471	0.0203	196.2	9.94×10^{-4}	45	Blended with CH ₃ CN
22 15 7 1 - 21 14 8 1	350450.9510	0.0203	196.2	9.94×10^{-4}	135	+ Absorption
22 15 7 0 - 21 14 8 0	350502.5773	0.0204	165.6	1.02×10^{-3}	45	Blended with CH ₂ OHCHO
22 15 8 0 - 21 14 7 0	350502.6386	0.0204	165.6	1.02×10^{-3}	135	
21 16 5 0 - 20 15 6 0	352806.0046	0.0170	164.3	1.19×10^{-3}	129	Blended with CH ₂ DCHO
21 16 6 0 - 20 15 5 0	352806.0050	0.0170	164.3	1.19×10^{-3}	43	
21 16 6 1 - 20 15 5 1	352896.1707	0.0169	195.1	1.16×10^{-3}	129	Blended with HNCO
21 16 5 1 - 20 15 6 1	352896.1707	0.0169	195.1	1.16×10^{-3}	43	+ Absorption
20 17 3 0 - 19 16 4 0	355022.2395	0.0174	164.0	1.37×10^{-3}	41	Blended with (CH ₂ OH) ₂
20 17 4 0 - 19 16 3 0	355022.2395	0.0174	164.0	1.37×10^{-3}	123	+ Absorption
20 17 3 1 - 19 16 4 1	355248.4955	0.0174	195.0	1.35×10^{-3}	123	Blended with CH ₃ COCH ₃
20 17 4 1 - 19 16 3 1	355248.4955	0.0174	195.0	1.35×10^{-3}	41	
19 18 2 0 - 18 17 1 0	357200.3403	0.0231	164.7	1.58×10^{-3}	39	Blended with CH ₃ CHO
19 18 1 0 - 18 17 2 0	357200.3403	0.0231	164.7	1.58×10^{-3}	117	
23 15 9 1 - 22 14 8 1	359038.5618	0.0238	205.9	1.01×10^{-3}	141	Absorption
23 15 8 1 - 22 14 9 1	359038.5787	0.0238	205.9	1.01×10^{-3}	47	
23 15 8 0 - 22 14 9 0	359134.3667	0.0239	175.3	1.04×10^{-3}	141	Blended with CH ₂ DOH
23 15 9 0 - 22 14 8 0	359134.6047	0.0239	175.3	1.04×10^{-3}	47	and CH ₃ CDO
22 16 6 0 - 21 15 7 0	361496.5122	0.0191	173.6	1.21×10^{-3}	45	Blended with (CH ₂ OH) ₂
22 16 7 0 - 21 15 6 0	361496.5152	0.0191	173.6	1.21×10^{-3}	135	

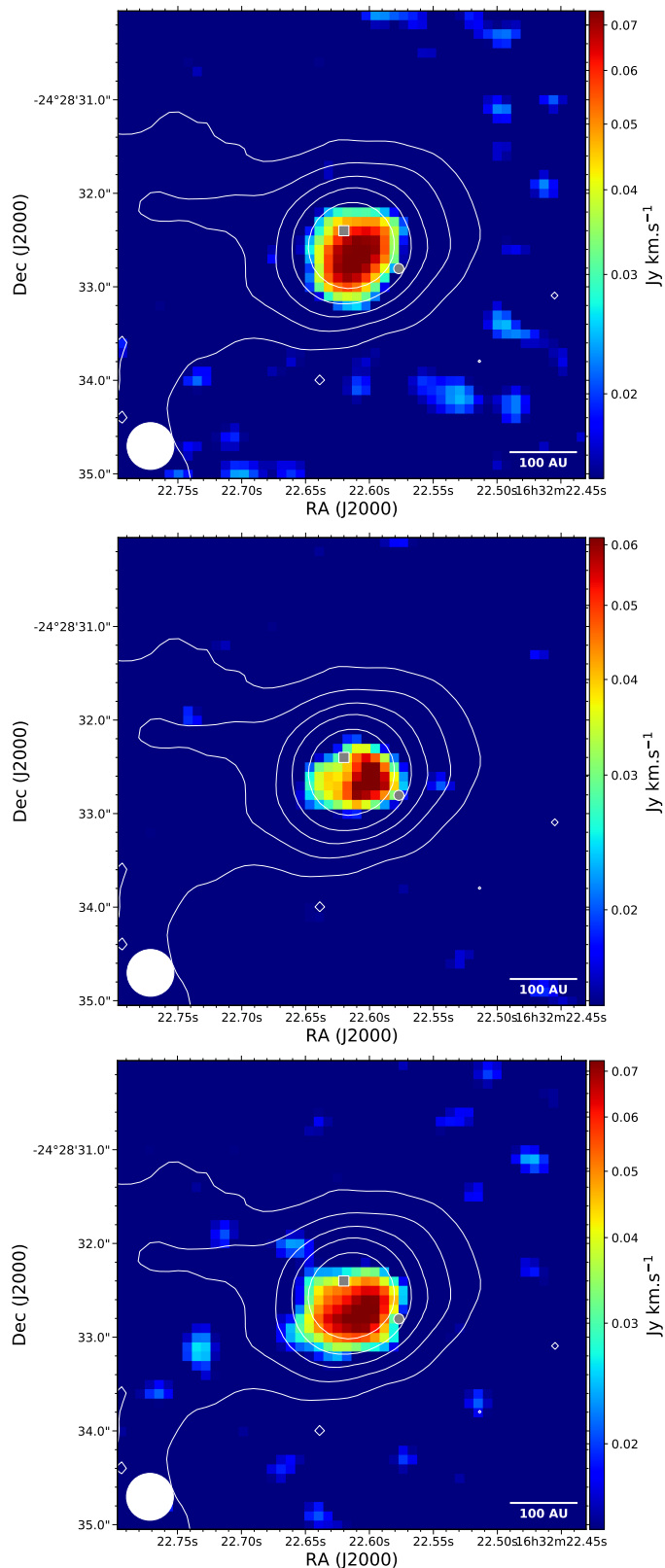


Fig. B.4. Integrated intensity maps of the HOCHCHCHO lines at 329.1843 (top), 330.8262 (middle), and 335.3758 GHz (bottom) towards IRAS16293 B. Dust continuum contours are indicated with white contours (levels of 0.02, 0.05, 0.1, 0.2, and 0.5 Jy beam⁻¹). The position of the continuum peak is indicated with a gray square, while the position analyzed for IRAS16293 B (full-beam offset) is indicated with a gray circle. The beam size is indicated in white in the bottom left corner.

Appendix C: Chemical modeling of 3-hydroxypropenal (HOCHCHCHO) and its isomers

HOCHCHCHO has a large number of isomers such as 2-propenoic acid (C_2H_3COOH), methyl glyoxal (CH_3COCHO), propanedial ($HCOCH_2CHO$), 2-hydroxypropenal ($CH_2COHCHO$), allenediol ($HOCHCCHOH$), vinyl formate (C_2H_3OCHO) and even cyclic compounds: β -propiolactone and oxiranecarboxaldehyde, with C_2H_3COOH the most stable isomer.

Complex molecules, such as the ones with a C_3 skeleton, are mainly produced through either: i) grain reactions of unsaturated molecules (C_3 , C_3H , C_3H_2 , C_3O , H_2C_3O , ...) initially produced in the gas phase then stuck on grains or ii) associations between radicals on grains (e.g., Harada et al. 2010; Garrod 2013; Garrod et al. 2017; Manigand et al. 2021). In the first case, the unsaturated molecules have to react on grains with O or OH to form molecules such as HOCHCHCHO and its isomers. As OH is not very mobile on grains and easily reacts with H_2 , only atomic oxygen through reactions with the C_3H_xO species can produce the isomers of $C_3H_4O_2$. However, O mainly reacts with the abundant radicals on the grains (HCO , CH_2OH , and CH_3O) and the production of $C_3H_4O_2$ isomers from the reactions of O is limited. In fact, only the isomer C_2H_3COOH is produced by this type of reaction in our network, with a rather low production.

In contrast to the $O + C_3H_xO$ reactions, the reactions with HCO are much more efficient because HCO is abundant and relatively mobile on the grains (Wakelam et al. 2017; Minissale et al. 2016). So, the reactions $HCO + C_2H_{x=1,3}O$ are efficient to produce (directly or after hydrogenation) the isomers of $C_3H_4O_2$ if the $C_2H_{x=1,3}O$ radicals are abundant. The $C_2H_{x=1}O$ ($HCCO$) is not very abundant on grains, according to our network, and thus it cannot be an important source of $C_3H_4O_2$. However, C_2H_3O radicals are quite abundant on grains, thereby leading to the formation of $C_3H_4O_2$.

Among the various C_2H_3O radicals, CH_3CO is the most abundant one. It is produced through addition of H on H_2CCO , but also through H atom abstraction of CH_3CHO and through the $CH_3 + CO$ reaction on grains. Besides CH_3CO , there are three other C_2H_3O radicals: CH_2CHO , CH_2COH , and $HCCHOH$; CH_2CHO is produced through the reaction $H_2CCO + H$ and through H atom abstraction of CH_3CHO . Furthermore, CH_2COH forms through addition of H on H_2CCO and H atom abstraction of C_2H_3OH , and $HCCHOH$ is produced by a H atom abstraction of C_2H_3OH .

The isomers of HOCHCHCHO are then formed according to the following reactions: CH_3COCHO (methyl glyoxal) is produced via the reaction $HCO + CH_3CO$. $HCOCH_2CHO$ (propanedial) is formed with the reaction between HCO and CH_2CHO which also produces (to a minor extent) C_2H_3OCHO (vinyl formate) because the single electron of CH_2CHO is partly delocalized on oxygen ($H_2C^{\bullet}-CH=O \longleftrightarrow H_2C=CH-O^{\bullet}$); $CH_2COHCHO$ (2-hydroxypropenal) results from the reactions between HCO and CH_2COH . The newly detected species, HOCHCHCHO (3-hydroxypropenal), can be produced by the reaction $HCO + CHCHOH$, but the abundance of $CHCHOH$ is low.

One important point is that methyl glyoxal/2-hydroxypropenal and 3-hydroxypropenal/propanedial are tautomeric couples. They are interconvertible by chemical reaction, in this case via a transfer of hydrogen atom (keto-enolic equilibrium). The reactions producing the $C_3H_4O_2$ isomers are exothermic. For example $HCO + CH_2CHO \rightarrow HCOCH_2CHO$ is exothermic

	$\Delta H_f^{\circ}K$ (kJ/mol)
2-propenoic acid (C_2H_3COOH)	-329 ^a -336.9 \pm 2.3 ^b
3-hydroxypropenal (HOCHCHCHO)	-286 ^a
Methyl glyoxal (CH_3COCHO)	-275 ^a -271.0 \pm 5.0 ^c
2-hydroxypropenal ($CH_2COHCHO$)	-268 ^a
Propanedial ($HCOCH_2CHO$)	-257 ^a
Vinyl formate (C_2H_3OCHO)	-255 ^a
TS for methyl glyoxal \rightarrow 2-hydroxypropenal	+6 ^a
TS for propanedial \rightarrow 3-hydroxypropenal	-23 ^a

Fig. C.1. Representation of the isomers of HOCHCHCHO included in the chemical modeling with their formation energies and the transition states (TS) between the tautomeric forms. The values with ^a are obtained through M06-2X/AVTZ calculations using $C_2H_4 + CO_2$ as a reference, while the ones with ^b and ^c refer to Guthrie (1978) and Moulds & Riley (1938), respectively.

mic by 306 kJ/mol. In this case, $HCOCH_2CHO$ is produced above the barrier to isomerization to HOCHCHCHO, located 72 kJ/mol below the $HCO + CH_2CHO$ entrance energy. The $HCOCH_2CHO$ with 306 kJ/mol of internal energy will relax through interaction with the ice. The typical timescale for isomeric conversion between $HCOCH_2CHO$ and HOCHCHCHO is shorter than for relaxation. Thus, as relaxation occurs, isomeric conversion leads to equilibrated isomeric abundances at each internal energy. The final balance is determined at or near the effective barrier to isomerization, which corresponds to

the energy of the transition state (Herbst et al. 2000), favoring HOCHCHCHO in that case. In our network, we consider that the ratio between the isomeric forms is then approximated by the ratio of the rovibrational densities of states of the isomers at the barrier to isomerization. For some reactions, the $C_3H_4O_2$ isomers are produced above dissociation limit and then some dissociate. The branching ratios towards dissociation are roughly estimated according to the excess energy above the dissociation limit and play a relatively small role in $C_3H_4O_2$ chemistry.

By considering the different reactions producing $C_3H_4O_2$, we introduced six of the isomers in our network: 3-hydroxypropenal (HOCHCHCHO), 2-propenoic acid (C_2H_3COOH), methyl glyoxal (CH_3COCHO), propanedial ($HCOCH_2CHO$), 2-hydroxypropenal ($CH_2COHCHO$), and vinyl formate (C_2H_3OCHO). These species are presented in Figure C.1 with their respective formation energies and the transition states between the tautomeric forms. The considered reactions can be found in Table C.1.

Table C.1. Reactions involved in the formation of the $C_3H_4O_2$ isomers.

Reaction	ΔE (kJ/mol)	Branching ratio	γ (K) (imaginary frequency)	Comments	
$C_3H_4O_2$ production					
HCO + CH_3CO	$\rightarrow CH_3COCHO$	-300	0.2	0	The TS for $CH_3COCHO \rightarrow CH_3CHO + CO$ is located 337 kJ/mol above the CH_3COCHO level so CH_3COCHO cannot dissociate. The TS for $CH_3COCHO \rightarrow CH_2COHCHO$ is located 281 kJ/mol above the CH_3COCHO level so CH_3COCHO can isomerize. However, CH_3COCHO should be favored. The TS for $CH_3CHO \rightarrow CH_4 + CO$ is located 354 kJ/mol above the CH_3CHO energy, so the CH_3CHO does not dissociate.
	$\rightarrow CH_2COHCHO$	-292	0.05	0	
	$\rightarrow CH_3CHO + CO$	-304	0.75	0	
	$\rightarrow H_2CCO + H_2CO$	-196	0	0	
	$\rightarrow CH_4 + CO + CO$	-322	0	0	
	$\rightarrow c-C_2H_4O + CO$	-204	0	0	
HCO + CH_2CHO	$\rightarrow HCOCH_2CHO$	-306	0.05	0	The TS for $HCOCH_2CHO \rightarrow HOCHCHCHO$ is located +234 kJ/mol above the $HOCH_2CHO$ level and the TS for $HCOCH_2CHO \rightarrow CH_3CHO + CO$ is located 301 kJ/mol above the $HOCH_2CHO$ level so $HOCH_2CHO$ can isomerize but mostly not dissociate. The lonely electron of CH_2CHO is localized on CH_2 (80%) site with a small but non negligible contribution to oxygen (20%). So, some C_2H_3OCHO should be produced.
	$\rightarrow HOCHCHCHO$	-335	0.2	0	
	$\rightarrow C_2H_3OCHO$	-303	0.02	0	
	$\rightarrow CH_3CHO + CO$	-328	0.73	0	
	$\rightarrow H_2CCO + H_2CO$	-220	0	0	
	$\rightarrow CH_4 + CO + CO$	-347	0	0	
HCO + CH_2COH	$\rightarrow CH_2COHCHO$	-408	0.05	0	The TS for $CH_2COHCHO \rightarrow CH_3COCHO$ is located 242 kJ/mol above the $CH_2COHCHO$ level so $CH_2COHCHO$ can isomerize. The TS for $CH_3COCHO \rightarrow CH_3CHO + CO$ is located 337 kJ/mol above the CH_3COCHO level, so CH_3COCHO can dissociate.
	$\rightarrow CH_3COCHO$	-416	0.2	0	
	$\rightarrow CH_3CHO + CO$	-481	0.75	0	
	$\rightarrow H_2CCO + H_2CO$	-312	0	0	
	$\rightarrow CH_4 + CO + CO$	-456	0	0	
HCO + $CHCHOH$	$\rightarrow HOCHCHCHO$	-444	0.2	0	The TS for $HOCHCHCHO \rightarrow HCOCH_2CHO$ is located 263 kJ/mol above the $HOCHCHCHO$ level so $HOCHCHCHO$ can isomerize but is favored. The TS for $HCOCH_2CHO \rightarrow CH_3CHO + CO$ is located 301 kJ/mol above the $HOCH_2CHO$ level so $HOCH_2CHO$ can dissociate.
	$\rightarrow HCOCH_2CHO$	-415	0.05	0	
	$\rightarrow C_2H_3OH + CO$	-396	0.75	0	
	$\rightarrow HCCOH + H_2CO$	-190	0	0	
	$\rightarrow CH_4 + CO + CO$	-456	0	0	
$C_3H_4O_2$ consumption					
H + C_2H_3COOH	$\rightarrow CH_3CHCOOH$	-176	1	1000(800i)	Barrier and imaginary frequency are guessed by comparison with similar reactions.
H + CH_3COCHO	$\rightarrow CH_3CO + CO + H_2$	-66	1	3400(1900i)	The barriers and imaginary frequencies are calculated at M06-2X/AVTZ level but for the moment we consider only one type of products to take into account the consumption without introducing all the $C_3H_5O_2$ isomers.
	$\rightarrow CH_3COCH_2O$	-89	0	2200(900i)	
	$\rightarrow CH_3COHCHO$	-201	0	3900(1200i)	
	$\rightarrow CH_3COCHOH$	-203	0	4150(1300i)	
H + HOCHCHCHO	$\rightarrow HOCH_2CHCHO$	-107	0	2900(840i)	The barriers and imaginary frequencies are calculated at M06-2X/AVTZ level but for the moment we consider only one type of products to take into account the consumption without introducing all the $C_3H_5O_2$ isomers.
	$\rightarrow HOCHCHCH_2O$	-19	0	4100(900i)	
	$\rightarrow HOCHCHCHOH$	-111	0	4000(1300i)	
	$\rightarrow HOCHCHCO + H_2$	-20	0	3100(1600i)	
	$\rightarrow CH_3CHO + HCO$	-88	1	3100(1600i)	
H + $HCOCH_2CHO$	$\rightarrow CH_3CHO + HCO$	-82	1	3000(1600i)	Barrier and imaginary frequency are guessed by comparison with similar reactions.
H + $CH_2COHCHO$	$\rightarrow CH_3COHCHO$	-209	0	1100(500i)	The barriers and imaginary frequencies are calculated at M06-2X/AVTZ level but for the moment we consider only one type of products to take into account the consumption without introducing all the $C_3H_5O_2$ isomers.
	$\rightarrow CH_3CHO + HCO$	-72	1	1100(500i)	
H + C_2H_3COCHO	$\rightarrow CH_3CHOCHO$	-150	0	800(630i)	The barriers and imaginary frequencies are calculated at M06-2X/AVTZ level but for the moment we consider only one type of products to take into account the consumption without introducing all the $C_3H_5O_2$ isomers.
	$\rightarrow CH_3CHO + HCO$	-85	1	800(630i)	

Table C.1. Continued.

Reaction	ΔE (kJ/mol)	Branching ratio	γ (K) (imaginary frequency)	Comments	
C ₂ H ₃ O production					
H + H ₂ CCO	→ CH ₃ CO	-165	0.1	2300(680i)	The barriers and imaginary frequencies are calculated at M06-2X/AVTZ level. The TS for CH ₃ CO → CH ₃ + CO is located 69 kJ/mol above the CH ₃ CO energy, so a large part of CH ₃ CO dissociates. The TS for CH ₂ CHO → CH ₃ CO is located 166 kJ/mol above the CH ₂ CHO energy and then CH ₂ CHO cannot isomerize. The TS for CH ₂ COH → CH ₂ CHO is located 139 kJ/mol above the CH ₂ COH energy, so CH ₂ COH cannot isomerize. See also Senosiain et al. (2006) and Michael et al. (1979) .
	→ CH ₃ + CO	-120	0.3	2300(680i)	
	→ CH ₂ CHO	-141	0.3	4030(930i)	
	→ CH ₂ COH	-49	0.3	7000(1600i)	
H + HCCOH	→ CH ₂ COH	-188	0.1	1840(680i)	The barriers and imaginary frequencies are calculated at M06-2X/AVTZ level. The TS for CH ₂ COH → CH ₂ CHO is located 139 kJ/mol above the CH ₂ COH energy, so most of the CH ₂ COH isomerize into CH ₂ CHO. The TS for CHCHOH → CH ₂ CHO is located 146 kJ/mol above the CHCHOH energy, and the TS for CHCHOH → CH ₂ COH is located 199 kJ/mol above the CHCHOH energy, so some CHCHOH isomerizes into CH ₂ CHO but not into CH ₂ COH.
	→ CHCHOH	-171	0.2	1920(770i)	
	→ CH ₂ CHO	-281	0.7	1840(680i)	
	→ H ₂ + HCCO	-129	0		
H + CH ₃ CHO	→ C ₂ H ₃ O	-69	0.25	3300(910i)	The barriers and imaginary frequencies are calculated at M06-2X/AVTZ level. See also Hippler & Viskolcz (2002) and Whytock et al. (1976) .
	→ CH ₃ CHOH	-110	0.25	5040(1360i)	
	→ CH ₃ CO + H ₂	-61	0.25	2400(1660i)	
	→ CH ₂ CHO + H ₂	-38	0.25	4900(1700i)	
CH ₂ + HCO	→ CO + CH ₃	-383	0.7	0	The TS for CH ₂ CHO → CH ₃ CO is located 166 kJ/mol above the CH ₂ CHO level, so -239 kJ/mol below the CH ₂ + HCO energy.
	→ CH ₂ CHO	-405	0.1	0	
	→ c-CH ₂ (O)CH	-266	0	0	
	→ CH ₃ CO	-429	0.1	0	
	→ H ₂ CCO + H	-264	0.1	0	
CH ₃ + CO	→ CH ₃ CO	-46	1	3500(420i)	The barrier and imaginary frequency is calculated at M06-2X/AVTZ level taking into account the previous results from Baulch et al. (2005) , Anastasi & Maw (1982) , Senosiain et al. (2006) , and Ding et al. (2001) .
O + C ₂ H ₃	→ CH ₂ CHO	-536	0.2	0	Deduced from Jung et al. (2015) .
	→ CH ₃ CO	-559	0.2	0	
	→ H ₂ CCO + H	-380	0.2	0	
	→ CH ₃ + CO	-512	0.4	0	
	→ C ₂ H ₂ + OH	-275	0	0	